Biochemical, structural and dynamical studies reveal strong differences in the thermal-dependent allosteric behavior of two extremophilic lactate dehydrogenases

Antonio Iorio, Jennifer Roche, Sylvain Engilberge, Nicolas Coquelle, Eric Girard, Fabio Sterpone, Dominique Madern

Biochemical, structural and dynamical studies reveal strong differences in the thermal-dependent allosteric behavior of two extremophilic lactate dehydrogenases.

Antonio Iorio[1], Jennifer Roche[2], Sylvain Engilberge[2,3], Nicolas Coquelle[4], Eric Girard[2], Fabio Sterpone[1]*and Dominique Madern[2]*

1- CNRS, Université de Paris, UPR 9080, Laboratoire de Biochimie Théorique, Paris, France; Institut de Biologie Physico-Chimique-Fondation Edmond de Rothschild, PSL Research University, Paris, France.

2-Univ. Grenoble Alpes, CEA, CNRS, IBS, 38000 Grenoble, France

3-Laboratory of Biomolecular Research, Division of Biology and Chemistry, Paul Scherrer Institut, 5232 Villigen, Switzerland

4-Large Scale Structures Group, Institut Laue-Langevin, 71 avenue des Martyrs, 38042 Cedex 9, Grenoble, France.

* Corresponding authors : Dr Dominique Madern, Dr Fabio Sterpone,

Email: dominique.madern @ ibs.fr; fabio.sterpone@ ibpc.

Keywords. Allosteric regulation; lactate dehydrogenase; conformational landscape; hyperthermophilic; molecular dynamics; quaternary structure.

Highlights

- Hyperthermophilic lactate dehydrogenases from *P. mobilis* and *T. thermophilus* display dramatic differences in thermal-dependent homotropic activation.
- Molecular dynamics simulation reveals how the thermally induced conformational landscape reorganizations influence allosteric behavior.
-Local dynamics of key amino acids modulate signal transition within lactate dehydrogenases.

Abstract.

In this work, we combined biochemical and structural investigations with molecular dynamics (MD) simulations to analyze the very different thermal-dependent allosteric behavior of two lactate dehydrogenases (LDH) from thermophilic bacteria. We found that the enzyme from *Petrotoga mobilis* (*P. mob*) necessitates an absolute requirement of the allosteric effector (fructose 1, 6-bisphosphate) to ensure functionality. In contrast, even without allosteric effector, the LDH from *Thermus thermophilus* (*T. the*) is functional when the temperature is raised. We report the crystal structure of *P. mob* LDH in the Apo state solved at 1.9 Å resolution. We used this structure and the one from *T. the*, obtained previously, as a starting point for MD simulations at various temperatures. We found clear differences between the thermal dynamics, which accounts for the behavior of the two enzymes. Our work demonstrates that, within an allosteric enzyme, some areas act as local gatekeepers of signal transmission, allowing the enzyme to populate either the T-inactive or the R-active states with different degrees of stringency.

1. Introduction

Allostery is a ubiquitous biological regulatory mechanism essential for cell growth and adaptation. The concept of allosteric regulation refers to the modification of the functional capacity of an enzyme through binding of a ligand at a specific site, distant from the active site. In the original paradigm, regulation relies on a ligand-dependent conformational change between a relaxed active state (R-state) and tense inactive state (T-state) (Monod et al., 1965; Koshland et al., 1966). Since the introduction of this concept, extensive investigations have shown that allostery is rooted in the dynamical properties of proteins, and the general "ensemble model" of allostery has been proposed (Motlagh et al., 2014; Wei et al., 2016; Wodak et al., 2019). According to this model, the allosteric behavior of an enzyme depends on the reorganization of its conformational landscape induced by different events such as interactions with other protein partners and ligands, local unfolding, reactive oxygen species and physico-chemical variations in the environment (Astl et al., 2020; Arai et al., 2010; Schrank et al., 2009; Halgand et al., 2020; Lisi et al., 2018). Temperature is a key environmental parameter with a major impact on conformational fluctuations and protein dynamics (Karshikoff et al., 2015; Kalimeri et al., 2013, Capdevila et al., 2017); therefore, understanding how temperature drives allosteric properties of an enzyme is of fundamental importance. To date, only a handful of studies addressed this issue (Bruzzese and Connelly, 1997; Fago et al., 2004; Sitzia et al., 2011; Colletier et al., 2012; Lisi et al., 2018; Katava et al., 2020).

Lactate dehydrogenases (LDH) (EC 1.1.1.27) belong to a wide group of 2-ketoacid: NAD(P)-dependent dehydrogenases that catalyze the reversible conversion of 2-hydroxyacids to the corresponding 2-ketoacids. LDHs are involved in energy metabolism and operate at the final stage of aerobic glycolysis (Holbrook et al., 1975; Ferst, 1985). LDHs have been used as models to study allosteric regulation. Most bacterial LDHs are tetrameric with a sigmoidal enzymatic activity profile, in the absence of fructose 1,6-bisphosphate (FBP),indicative of a homotropic activation effect of the substrate on the reaction. In the presence of FBP, their enzymatic activity profiles become hyperbolic, demonstrating heterotropic allosteric activation (Schroeder et al., 1988; Arai et al., 2002; Feldman-Salit et al., 2013; Taguchi, 2017). In contrast, vertebrate LDHs are considered as non-allosteric, even if some studies suggested reminiscent allosteric properties (Katava et al., 2017). When the competent catalytic state is reached, LDH catalyzes the direct transfer of a hydride ion from the pro-R face of NADH to the C2 carbon of pyruvate to produce lactate (Burgner et al., 1984; Clarke et al., 1986; Clarke et al., 1988; Deng e al., 2011).

Abundant structural information has been obtained from crystal structures of allostericand non-allosteric LDHs with ligands (Holo) and without (Apo) (Kolappan et al., 2015; Matoba et al., 2014; Arai et al., 2010; Coquelle et al., 2007; Winter et al., 2003; Auerbach et al., 1998; Iwata et al., 1994, Piontek et al., 1990). The four subunits of LDHs are related by three molecular 2-fold axes named P, Q, and R. The active site of each subunit lies near the Q-axis interface (Rossmann et al., 1973). Crystallographic structures of allosteric LDHs revealed in detail the binding mode of the cofactor (NADH), the substrate (pyruvate) and the FBP (Wigley et al., 1992; Iwata et al., 1994; Coquelle et al., 2007). The tetramers of allosteric LDHs have four active sites and two FBP-binding sites. Pyruvate is a keto acid recognized within the catalytic site by the positively charged lateral chain of Arg 171, universally conserved in LDHs (numbering follows the LDH nomenclature from (Eventoff et al., 1977)). Upon formation of the transition state, the active site loop covers the catalytic site allowing its dehydration and the correct anchoring of the substrate (Wigley et al., 1992; Iwata et al., 1994; Coquelle et al., 2007). In allosteric LDHs, other structural reorganizations take place, which involve changes such as the compaction or the expansion of the quaternary assembly together with some helix sliding and local rearrangement of the catalytic site (Reviewed by Taguchi, 2017)

While previous studies using LDHs from different thermally adapted organisms have revealed the key role that protein flexibility plays in protein adaptation (Coquelle et al., 2007, Colletier et al., 2012, Peng et al., 2015), a full understanding of how this translates into the control of functionality is still un clear. In order to gain insight into the effect of temperature on allosteric regulation, the present study reports a detail investigation of two LDHs from thermophilic bacteria, the *Thermus thermophilus* (*T. the*) from the Deinococcus-Themus phylum, and the *Petrotoga mobilis* (*P. mob*) a species of the *Thermotogae* phylum, which display a similar optimum temperature for growth (OTG), 65°C, (Oshima and Imahori, 1974, Lien et al., 1988) but, as we demonstrate, a different mode of enzymatic activity control.

The manuscript is organized as follows. We first show the different activity profiles of the two homologues as a function of temperature and in presence or not of the allosteric effector FBP. The x-ray structure of *P. mob* LDH is reported here and compared with the one of *T. the* to identify possible structural features explaining the activity profiles. We then rationalize this behavior by considering static structural features of the two enzymes by comparing the existing x-ray structure for *T. the* LDH with the x-ray structure of *P. mob* LD, solved and presented in this work. We finally consider the effect of temperature on the protein conformational states relevant for the enzyme functionality using MD simulations.

2. Results.

In order to facilitate comparison a dual numbering system was used for enzyme residues. It combines the linear numbering based on the primary sequence of each LDH with the normalized numbering for LDHs, useful for structural comparison (Eventoff et al., 1977). A sequence alignment between *P. mob* and *T. the* LDHs is presented in Figure S1.

Quaternary assembly of *P. mob* LDH in solution.

Elution profiles of the purified *P. mob* LDH on a size exclusion chromatography column is shown in Figure S2. For the main peak, the experimental weight-averaged molecular mass measured by combining on line Multi-Angle Laser Light Scattering (MALLS) and differential refractive index measurements was121 ± 6 kDa, in agreement with the theoretical molecular weight of 133 for a tetrameric association. The second peak with a molecular mass of 248 kDa suggests the presence of an octamer.

Effect of temperature on homotropic and heterotropic allosteric activation.

We recorded the catalytic properties of *P. Mob* and *T. the* LDHs at pH 6.0 at both 50°C and 70°C (Figure 1). In absence of FBP, the pyruvate saturation profile of *P. mob* LDH shows the enzyme is virtually inactive, irrespective of the temperature, (Figure 1 (A) and (C)). This indicates that the enzyme is mainly in the T-inactive state. In contrast, *T. the* LDH is active, at the same temperature, with a bell-shape profile demonstrating a phenomenon of inhibition by high substrate concentration typical of numerous LDHs (Figure 1 (E) and (G)). Kinetics parameters for *T. the* LDH show the specific activity at 70°C increases and the K_m values drops to 0.11 mM (Table 1). This indicates that the temperature increase induces a favorable change of substrate affinity in *T. the* LDH.

When supplemented with FBP, activity profiles of *P. mob* LDH (Figure 1(B) and (D)) show the enzyme is activated at both temperatures demonstrating strong heterotropic activation. At 50°C, high concentration of substrate inhibits *P. mob* LDH activity (Figure 1 (B)). At 70°C, the activity values are similar over the pyruvate concentration range of 5-90 mM showing that temperature increase has abolished the inhibition by high concentration of substrate in the presence of FBP (Figure 1 (D). With *T. the* LDH, however, addition of FBP did not induce significant activity profiles ((Figure 1 (F) and (H)) compared to those recorded without allosteric effector (Figure 1 (E) and (G)). At 70°C, the specific activity of *P. mob* LDH increases

to 939 U/mg and K_m value for pyruvatedecreasesfrom0.65 to 0.17 mM (Table 1). With *T. the* LDH in the presence of FBP, K_m values for pyruvate are low at both temperatures. Rising the temperature increases activity from 109 to 433 U/mg. At 70°C in the presence of FBP, values of V_{max}/K_m for *P. mob* and *T. the* LDH indicate a similarly high catalytic efficiency.
Our data demonstrate that *P. mob* and *T. the* LDHs display strong differences with respect to the effect of temperature on homotropic activation, whereas in the presence of FBP and at high temperature, both enzymes behave similarly.

Crystallographic structure of *P. mob* LDH.

We determined the crystal structure of the *P. mob* LDH binary complex with NADH. Data collection and refinement statistics are summarized in Table S1. *P. mob* LDH crystallizes in the space group *C*121 with a dimer in the asymmetric unit (PDB accession code: 6H9S). The final tetrameric structure of *P. mob* LDH, corresponding to the solution structure determined by SEC-MALLS, is shown in Figure 2(A).

Subunit contacts that maintain the tetrameric state occur through interfaces along the P, Q and R axes (Figure 2(B)). The *P. mob* LDH monomer displays the typical fold of homologs belonging to the lactate and malate dehydrogenase family (Conserved protein domain family, accession cd05292). Residues 1-138 form the NAD(P)-binding Rossmann-fold domain and residues 139-307define the substrate-binding site in the C-terminal domain. In both monomers, two areas between residues 79-83 and 195-205 are of weak electron density preventing their modeling. In LDHs, the first region corresponds to the mobile loop that covers the active site upon substrate binding (Iwata et al., 1994; Coquelle et al., 2007). Because of its high flexibility, this area is frequently not defined in LDHs crystal structures. The other region corresponds to a contact area between the P-axis related subunits.

Structural comparison between *P. mob* and *T. the* LDHs.

We compared the structures of *P. mob* and *T. the* LDHs considering known structural features associated with the allosteric behavior of LDHs (Taguschi, 2017). Structures of the *T. The* LDH were solved in both T-inactive and R-active states (*T. the* LDH, accession codes 2V6M and 2V7P, respectively). The lower RMSD values obtained between *P. mob* LDH (6H9S) and 2V6M (2.3 Å) compared to the one between 6H9S and 2V7P (3.0 Å) indicates *P. mob* LDH in binary complex and the Apo T-inactive state of *T. the* LDH are structurally closer. Studies on LDHs and MalDHs have shown that the formation of the binary complex with

NADH induces negligible structural reorganization compared to the Apo state (Gonzalez et al., 2018 and reference therein). In allosteric LDHs, homotropic and heterotropic activations are due to the binding of the substrate and the allosteric effector (FBP), respectively. These induce major structural reorganizations including helix sliding and a compaction of the tetramer (Reviewed by Taguschi, 2017). These reorganizations allow the lateral chain of the universally conserved substrate-binding residues R148(171) to enter within the catalytic site (Iwata et al., 1994; Coquelle et al., 2007; Colletier et al., 2012, Ikehara et al., 2014).This situation explains the increase of affinity for pyruvate in the activated (R-state). In order to identify structural features that might explain the biochemical differences observed between *P. mob* and *T. the* LDHs, a comparison between several groups of amino acids considered as playing an important role in allosteric behavior is presented below. A series of interactions form a "communication network" between the FBP-binding site (FBPbs) and the substrate binding residue R148(171) (Figure 3).

The *P. mob* LDH crystal structure shows that the local topology of R148(171) is outside the catalytic site and corresponds to the expected position for a T-inactive state as it is the case with the Apo structure of *T. the* LDH (Figure 3(B) and (C)) and for other allosteric LDH structures in the Apo state. Note, that in allosteric LDHs, the lateral chain movements of R148(171) and H47(68) of the adjacent monomer at the Q related interface are coordinated (Iwata et al., 1994; Coquelle et al., 2007, Colletier et al., 2012; Ikehara et al., 2014). In *P. mob* and *T. the* LDHs, there is no significant difference in the topology of these two conserved amino acids (Figure 3(B) and (C)). However, the absence of homotropic activation in *P. mob* LDH strongly suggests that this area located at the Q related interface is not flexible enough, even at high temperature, preventing the lateral chain ofR148(171) from accessing the active site. In contrast, the activation profiles for *T. the* LDH showing that the enzyme is activated by high temperature without FBP suggests that the energetic barrier, which prevents the entry of the lateral chain of R148(171) within the catalytic site, is lowered by temperature. A situation allowing the lateral chain of R171 to enter into the catalytic site.

In allosteric tetrameric LDHs, FBP binding triggers heterotropic activation. Crystal structures show that two FBP bind between monomer A and D at the P-related interface (Iwata et al., 1994; Ikehara et al., 2014). The effectors are anchored by a set of residues including R150(173), H165(H188) and Y167(190) from both monomers forming FBPbs. In *P. mob*, as well as in *T. the* LDH, these three residues are conserved. Several studies on allosteric LDHs have underpinned the major role of H165(188) in FBP binding (Schroeder et al., 1988). Crystal

structures of different LDHs from *Thermus* species, *T. thermophilus* (Apo form, 2V6M and Holo form, 2V7P) and *T. caldophilus* (*T. cal*) (Holo form, 3VPH) show that H188 lateral chain occupies different positions that are specific for T- or R-states. In the R-active state of *T. cal* LDH the two imidazolium rings are positioned parallel to each other to accommodate the FBP (Ikehara et al., 2014). Within *T. the* LDH (2V7P) in the R-active state, H188 occupies a similar position although it holds no FBP (Coquelle et al., 2007). H188 conformation in the Apo state of *T. the* LDH is typical of the T-inactive state (Figure 3(I)). In the Apo *P. mob* LDH structure, H165(188) lateral chain is very flexible and visits two conformational sub states that correspond to the position encountered in either the Apo or Holo structures of allosteric LDHs including those of *T. the* LDH (Figure 3(H)). In the most extended sub state, the distance between CG atom of two H165(188) is (~8.1Å), whereas it is (~ 4.8 Å) in the sub state mimicking the one encountered within the R-active state of LDHs when liganded with FBP.

The FBPbs interacts with another area playing a major role in the allosteric behavior of LDHs (Taguchi, 2017). This area, the allosteric core (Alco), is a hydrophobic-rich area, which "mechanically" links the FBPbs to the substrate binding residue R148(171) (Ikehara et al., 2014). Alco constitutes a rigid mobile body for the allosteric motion in LDHs from *Thermus* species (Ikehara et al., 2014). Interface between FBPbs and Alco involves residues 182(205), 184(207), 186(209), 187(210) (Figure 3(F) and (G)). In this area, *P. mob* LDH differs from *T. the* LDH by a single amino acid replacement M184(207) to Q. Alco is defined by positions 148(171), 149(172), 150(173), 153(176), 167(190), 168(191), 178(201) and W180(203) (Figure 3(D) and (E)). R148(171) position in the substrate binding site is thus directly influenced by interactions within Alco. Allosteric core comparison, between *P. mob* and *T. the* LDHs, reveals that there is some differences in the local topology due to changes in amino acid composition. In *T. the* LDH, R171 is connected to Alco owing to the lateral chain of the neighboring amino acid F172. The side chain of F172 interacts with those from L176, L201 and W203. In *P. Mob* LDH there is a complete local reorganization due to amino acid replacements i.e. L149(172), I153(176) and A178(L201). Consequently, the lateral chain of W180(203) in *P. mob* LDH slightly flip by 15 degrees compared to *T. the* LDH (Figure 3 (D) and (E)).

Allosteric activation of enzymes relies on the capacity to transmit a signal through a network of contacts from a binding-site distant from the substrate binding-site. The present work shows clear differences between the thermally dependent allosteric properties of *P. mob* and *T. the* LDHs. Their crystal structures show they share a common fold. In each enzyme, the

lateral chain of their substrate-binding residues R148(171) is in the T-inactive position. Even if some variations are observed in the network of contacts in the vicinity of R148(171), the structural comparison fails to provide a satisfactory explanation to account for the thermal-dependent enzymatic differences. Recent models of allostery emphasize the role of dynamics, the ensemble nature and ligand induced population shifts (Swain et al., 2006; Goodey et al., 2008; Motlagh et al., 2012; Motlagh et al., 2014). In order to decipher how the presence of the allosteric effector or the change in temperature control the conformational landscape of the two enzymes we performed atomistic MD simulations, presented in the following sections.

Effect of temperature on conformational landscapes of *P. mob* and *T. the* LDHs

In order to grasp the effect of temperature on the protein matrix fluctuations, and therefore to characterize the proteins conformational landscape, we performed a series of MD simulations of the two proteins in both the Apo and Holo models. Indeed, MD simulations have been proven to be very effective for inspecting the relationship among protein conformational flexibility, stability and optimal functionality (Sterpone et al., 2009; Sterpone and Melchionna 2012; Katava et al., 2016; Katava et al., 2017; Katava et al., 2020; Maffucci et al., 2020). We first analyzed the formation of salt bridges that are considered as important structural features playing a role in thermal adaptation and found no major differences between the two enzymes, see Figure S3 and Table S2.

Then, we analyzed the proteins in the Apo state at different temperatures. In order to individuate the conformational states accessed by each monomer, a clustering of the sampled configurations was performed. The resulting conformations were further grouped in kinetically relevant states using a Markov clustering algorithm. This approach allows connecting the conformations that actually can dynamically inter-convert one into each other.

For clarity, we only report the data for one monomer of the tetramer (monomer D). The analysis was also done for the other monomers and the results were similar. The results of the clustering procedure on the entire monomer D, for both *T. the* and *P. mob* at 300 K and 340 K are represented in the form of a network of interconnected configurational states (Figure 4(A)).

Two main features emerge. First, the *P. mob* LDH monomer is systematically more flexible – visits more states-than the *T. the* LDH monomer. When the temperature rises from 300 to 340 K, the number of sub states inflates from 15 to ~200 in the *P. mob* LDH monomer, whereas it increases from 6 to 91 with *T. the* LDH (Figure 4(A)). Secondly, the structure of the conformational landscape is much more compact in *T. the* LDH, with conformations that, in

the kinetic space, remain closer to each other. The conformational entropy associated with the protein landscape is quantified in Figure 4(B).We represent the effect of temperature on the estimated total number of clusters visited by the two proteins domains ($N\infty$),and on the number of states that are kinetically connected (N_K) (Kalimeri et al., 2013). In both cases, *P. mob* LDH outperforms *T. the* LDH. These findings indicate that the monomers of *T. the* LDH are more resilient to temperature stress, and more rigid from the conformational point of view.

In order to get a clearer insight on the relationship among structure, fluctuations, dynamics and function, we specifically focused on two key local elements of the structure. The first concerns the orientation of the substrate-binding residue R148(R171). In general, the crystallographic structures of allosteric LDHs reveal two different positions of this residue when passing from Apo (representative of the T-inactive) to Holo (representative of the R-active) states (Reviewed by Taguchi 2017). We were able to explore the dynamics of this residue and single out the different orientations it can adopt. In particular, we were interested to verify the capability of R148(171) to sample the functional orientation when its positively charged side chain points inwards in the catalytic site to support the binding of the substrate through an interaction with the negatively charged extremity of the pyruvate. For each configuration generated along the MD trajectory, we computed the RMSD with respect to the Apo structures of *P. mob* and *T. the* LDH X-ray structures and to the homology model and X-ray structure of *P. mob* and *T. the* enzyme in the Holo states, respectively. The RMSD were computed on all the atoms of the R148(171) residue. We present the obtained density map in this reduced two-dimensional space (Figure 5).

At ambient temperature (300K) for *P. mob* LDH, R148(171) samples a restricted ensemble of orientations within a main structural basin close to the X-ray structure ($RMSD_A$ of 0.5 Å) and hardly approaches the Holo configuration based on the homology model ($RMSD_H$ of 1.9 Å) (Figure 5(A) top). Note that when the Holo structure of *T. the* LDH is taken as reference, the result is the same. Temperature increase does not alter significantly the distribution (Figure 5(A) bottom). The observation that the lateral chain of R148(171) stays in the T-state is in agreement with the enzymatic measurement showing that homotropic activation does not exist in *P. mob* LDH, irrespective of temperature. In contrast, for *T. the* LDH, R148(171) samples a broad ensemble of orientations within a main structural basin slightly deviating from the Apo X-ray structure ($RMSD_A$ of 0.5 Å), nevertheless approaching the Holo configuration ($RMSD_H$ 1.2-1.5 Å) (Figure 5(B) top). This proximity is further enhanced when considering the higher temperature close to the functional regime (Figure 5(B) bottom). This result is a first indication

that *T. the* LDH exhibits an intrinsic capability -reinforced by temperature- to explore functional configurations, which in allosteric LDHs are induced by the presence of the substrate or FBP.

We conclude our analysis by focusing now on two important structural regions that were described in Figure 3. The previous structural comparison suggested that the allosteric core (Alco) and the FBP-binding site, which are intrinsically related, display some differences that would affect the allosteric properties of the enzymes.

In order to capture their respective conformational flexibilities, these two regions were used for clustering analysis (Figure 6). The set of amino acids from the Alco is more rigid in *T. the* LDH than in *P. mob* LDH*i.e.* the number of configurational asymptotic clusters is lower for *T. the* LDH (Figure 6 (B)). Assuming that a rigid/compact region transfers a mechanical perturbation with low dissipation, our result suggests that in *T. the* LDH the allosteric core seems more effective for conformational change communication at long-range distance. On the contrary, the *T. the* LDH FBPbs region samples a larger number of conformations (high number of configurational asymptotic clusters at all temperatures), and thus is more flexible than the same region in *P. mob* LDH (Figure 6 (D)). We concluded the MD simulations with the interrogation of the relative distance between the residues H165(188) belonging to adjacent monomers at the P-axis related interface. In each monomer, H165(188) is an essential amino acid involved in the FBP binding. MD trajectories were used to explore the relative distances of these residues in the Apo LDHs. Interestingly, these trajectories evolve differently in the two proteins.

Consider first the AD and BC interfaces of *P. mob* LDH, where at ambient conditions the relative distance distribution sampled by the H165(188) pairs shows a peak (Figure 7 (A)), roughly corresponding to an intermediate position between the two alternate positions observed in the Apo structure.

These two positions correspond to conformational sub states observed in representative LDH crystal structures of Apo and Holo states complexed with FBP. When the temperature is raised close to the functional regime, T=340K, in *P. mob* LDH the distribution becomes broader expanding toward larger values, (Figure 7(B)), indicating that the H165(188) pairs sample more frequently the typical conformational sub state observed in the T-inactive form of LDHs. In contrast, in *T. the* LDH at 340 K, the distribution remains more compact with a lowest propensity to explore conformational sub states representative of the X-ray Apo configuration. The same analysis was done using measurements of distance between NG1 atoms in Figure S4. With *P. mob* LDH, the distribution profiles are strongly impacted, whereas those of *T. the* LDH are less sensitive. This indicates that the thermally induced change of H165(188) flexibility in *P. mob* LDH, is also due to a greater rotation capacity of the imidazole ring.

Again, this finding appears to confirm that when temperature effects on the conformational landscape are taken into account, the *T. the* LDH in the Apo state shows a propensity to sample functional-close conformations, while for the Apo *P. Mob* LDH the temperature has a more degrading functional effect. This represents an important structural support to the biochemical characterization showing that *T. the* LDH might be activated without allosteric effector while *P. mob* LDH cannot (Figure 1).

Conclusion

The behavior of allosteric bacterial LDHs fit the Monod-Wyman-Changeux transition model, which stipulates that the T-inactive and R-active states of an enzyme coexist independently of allosteric effectors (Taguchi, 2017).It implies that the T/R equilibrium is sensitive to any chemical-physical perturbation of the environment. Here, we report that the effect on the equilibrium of elevating the temperature is dramatically different for two LDHs from thermophilic bacteria. A pictorial representation of the main results on the features relating structure, function and conformational dynamics is shown in (Figure 8)). The data reveal that there is a single mechanism (FBP activation) for the enzyme from *P. mobilis* to switch to the active state, whereas in the enzyme from *T. thermophilus* the control of this transition is less stringent allowing the temperature to activate the enzyme even without effector. This observation implies that the transmission efficiency of the allosteric signal, via networks of interactions, allowing the catalytic site to be competent for functionality is different in these LDHs.

Based on a simple assumption that the shorter the path the better the transmission, we focused our analysis on the Alco area located between the FBPbs and the universally conserved substrate binding residue R148(171). MD simulations at various temperatures establish that Alco dynamics orchestrates (as an internal switch) the capacity of R148(171) to explore functional states. We propose that a rigid Alco is an efficient feature for signal transmission at long-range distance toward a catalytic site. This may propagate information induced not only by effector binding but also provoked by thermal agitation or by various other chemical-physical constraints. On the contrary, a more flexible Alco favors a more stringent regulation of activity allowing an allosteric enzyme to remain in the T-inactive state; the shift toward the functional state being induced only by effector binding, as exemplified with *P. mob* LDH.

Our findings give support to the hypothesis that the local entropy of hydrophobic cores, which undergo substantial structural fluctuations despites their high packing fraction, mediates

activation and regulation of enzymes (Van Vliet et al., 1991; Bowman and Geissler, 2014; Kim et al., 2017; Rajasekaran et al., 2017). Site-directed mutagenesis experiments are underway to characterize in detail Alco properties of thermophilic LDHs. It is worth noting that in *T. the* LDH the area defined as representative of the FBP binding site is able to sample more conformations than in *P. mob* LDH. This flexibility, however, does not affect the key inter monomer distances between the residues H165(188), a proxy for the FBP induced conformational changes, that remains in *T. the* LDH closer to the functional reference conformation even at high temperature. In *P. mob* LDH temperature increase clearly degrades this inter monomer connectivity, and drives the protein matrix far from the functional conformation that is recovered only with FBP binding. Therefore, we suggest that in *T. the* LDH the flexibility of the FBP binding region provides a channel to dissipate thermal energy to avoid the corruption of the essential inter monomer distances.

To conclude, the present work reveals that the fine dynamical interplay between different areas considered as local gatekeepers of signal transmission is of major importance to define allosteric properties of an enzyme.

4. Materials and methods

4.1. Cloning of P. mob LDH.

A gene encoding the lactate dehydrogenase of *P. mobilis* (NCBI Reference Sequence: WP_012209677.1) with codons optimized for expression in *Escherichia coli* was synthetized and sub cloned into pET-20a by Gencust. The *NdeI* and *BamHI* cloning sites were used for cloning.

4.2. Protein expression and purification.

E. coli BL21 DE3 competent cells transformed with pET-20 expression vector encoding *P. mob* LDH gene were selected by growth on LB agar plates containing 100 µg.mL^{-1} ampicillin. A single colony was grown overnight at 37°C in 50 mL LB medium at the same concentration of antibiotic. 20 mL of these cultures were then used for inoculation of a 2 liter LB medium containing 100 µg.mL^{-1} ampicillin. The cells were cultivated at 37°C until an OD_{600} of 0.6 was reached. Isopropyl B-D-1-thiogalactopyranoside (IPTG) was added at a final concentration of 0.5mM to induce expression and the culture was incubated for 4 hours at 37°C. Bacterial cells were harvested by centrifugation at 6000 g for 20 min at 4°C. The pellet was

suspended in 40 mL of 50 mM Tris-HCl pH 7.4 containing 50 mM NaCl (Buffer A). Prior cell disruption, 5 µg.mL^{-1} of DNAse and $MgCl_2$ to final concentration of 10mMwas added to the cell suspension. The preparation was cooled at 4°C and lysed by sonication (Branson sonicator). Six cycles of continuous sonication at 50 % amplitude were applied during 30 s. Between each pulse, the solution was kept on ice for one minute. The extract was then centrifuged at 13000 g for 30 min at 4°C. The supernatant was further incubated at 70°C for 30 min and the thermally unfolded proteins were removed by centrifugation. The extract was loaded on a Q sepharose column (2x10 cm) equilibrated with Buffer A. *P. mob* LDH was eluted with a linear gradient from 0 to 0.8 M NaCl in Buffer A. The active fractions containing the enzyme were pooled, concentrated and loaded on a Superpose 12 gel-filtration column (GE Healthcare) and eluted with Buffer A. The purity of the enzyme was checked by SDS gel electrophoresis. The enzyme was concentrated at 20 mg mL^{-1} in Buffer A and stored at 4°C. *T. The* LDH purification was done as previously described (Coquelle et al., 2007).

4.3. Size Exclusion Chromatography - Multi Angle Laser Light scattering (SEC-MALLS)

SEC combined with online detection by MALLS and refractometry (RI) was used to measure the absolute molecular mass of *P. mob* LDH in solution. The SEC run was performed using an ENrich^{TM} SEC650 10x300 gel-filtration column (Biorad) equilibrated with a buffer composed of 50 mM Tris-HCl pH7.2 and 50 mM NaCl. Separation was performed at room temperature and 50 µL of protein sample, concentrated at ~5 mg.mL^{-1}, was injected with a constant flow rate of 0.5 mL.min^{-1}. Online MALLS detection was performed with a DAWN-HELEOS II detector (Wyatt Technology Corp.) using a laser emitting at 690 nm. Protein concentration was determined by measuring the differential refractive index online using an Optilab T-rEX detector (Wyatt Technology Corp.) with a refractive index increment *dn/dc* of 0.185 ml^{-1} g^{-1}. Weight-averaged molecular weight (Mw) determination was done with the ASTRA6 software (Wyatt Technologies) and curve was represented with GraphPad Prism.

4.4. Enzymatic assay and protein determination

The activity of *P. mob* and *T. the* LDHs for reduction of pyruvate to lactate was carried out at 50 and 70°C in 500 µL of 2-(N-morpholino) ethane sulfonic acid (MES) pH 6.0 and supplemented with 50 mM NaCl. The reaction was monitored spectrophotometrically at 340 nm by following the oxidation of NADH (0.5mM) on a Jasco 540. To record the enzymatic profile of both enzymes, various substrate concentrations were tested with or without addition of fructose 1,6-bis-phosphate (FBP). The data were analyzed using Michaelis-Menten or

allosteric sigmoidal equations in GraphPad Prism version 7.03. The protein concentration was estimated from the absorbance at 280 nm using a Nanodrop 2000 (Thermo Scientific), with molecular weight and extinction coefficient calculated using the server https://web.expasy.org/protparam.

4.5. Crystallization and structure determination

An initial crystallization screening of *P. mob* LDH was performed at 20°C using a robotic crystallization system (https://htxlab.embl.fr). The protein concentration was 10 mg.mL^{-1} in the following buffer: 50mM Tris-HCl pH7, 50 mM NaCl, 2mM NADH and 10 mMTb-Xo4 crystallophore™ (Engilberge et al., 2017, Engilberge et al., 2018).The optimized crystallization solution contains 20% PEG 3350 and 100 mM $NaNO_3$. The crystals grew in 24 hours using the hanging drop vApor diffusion method. The drops were done by mixing 1.5 µL of the protein solution with 1.5 µL of the crystallization solution. The crystals were harvested, soaked in a cryo protection solution and flash-frozen in liquid nitrogen. The cryo protection solution was the mother liquor containing 20% of glycerol.

P. mob LDH diffraction data were collected on the ID30A-1 MASSIF-1beamlineat the European Synchrotron Radiation Facility (ESRF) (Grenoble, France). Data sets were indexed and integrated using XDS (Kabsch, 2010). Scaling, density modification and molecular replacement were done with the CPP4 suite using SCALA (Evans, 2006), DM (Cowtan, 1999) and PHASER (McCoy et al., 2007), respectively. The model used for molecular replacement was the structure of *Thermotoga maritima* LDH (RCSB PDB accession code: 1A5Z). The structure was refined with multiple cycles of manual building using COOT (Emsley et al., 2010) and of refinement using phenix.refine (PHENIX suite, Afonine et al., 2012) and BUSTER (https://www.globalphasing.com/buster). The TLSMD server http://skuld.bmsc.washington.edu/~tlsmd/ (Painter and Merritt, 2005; Painter and Merritt, 2006) was used to generate TLS groups. Model quality was validated with MolProbity (http://molprobity.biochem.duke.edu) (Davis et al., 2007; Chen et al., 2010) and wwPDB validation service (https://validate-rcsb-1.wwpdb.org) (Berman et al., 2003).

The table of data collection and refinement statistics in (Table S1) was obtained using phenix.table-one (PHENIX suite).

4.6 Homology model building.

In the final crystallographic structure (6H9S) two small regions corresponding to residues 79-83 and 195-205 are not modeled. Accordingly, to perform MD simulations, which

require complete structural models (*i.e* without any missing residues or atoms) we used homology model building to reconstruct these two small areas.

Completion of models. To satisfy the above criterion, a complete model of *P. mob* LDH was generated using the Swiss model server (https://swiss model.expasy.org/) (Waterhouse et al., 2018), which includes the two loops missing in the crystallographic structure. This complete tetrameric homology based model was then superimposed onto each of the four monomers of the crystallographic structure forming the biological tetramer. Careful inspection of the crystallographic structure and the homology model did not reveal significant differences, in equivalent area. In the crystallographic structure of both the Apo and Holo states of *T. the* LDH (2V6M and 2V7P), a mobile loop is not defined in one monomer. Consequently, homology based models of *T. the* LDH in each states were generated using the same procedure.

Generation of Holo model of P. *mob* LDH.A model of the *P. mob* LDH ternary complex (with NADH and the substrate analog oxamate) was generated with I-TASSER server (https://zhanglab.ccmb.med.umich.edu/I-TASSER/) (Yang and Zang, 2015). Based on confidence scores, the server provided a Holo form of *P. mob* LDH using crystallographic structure of *T. the* complexed with NADH and oxamate (pdb id 2V7P).In the resulting Holo *P. mob* model, a single polypeptidic chain, including only the NADH, was generated. This model was superimposed with each of the four subunits of the tetrameric crystallographic structure of *T. the* LDH (pdb id 2V7P), with for example, an overall RMSD of 0.55 Å after superimposition with all the main-chain atoms of the chain A (0.65, 0.57 and 0.69 Å for the chains B, C and D, respectively). The oxamate molecules were finally added in each of the four subunits of the Holo *P. mob* model, using their respective positions in the crystallographic *T. the* LDH structure. After application of these different procedures, we produced a complete relevant set of structural models for each enzyme without missing area.

4.7 Molecular Dynamics.

We performed all-atom Molecular Dynamics simulations of tetrameric assembly models for *T. the* and *P. mob* LDHs constructed via homology modeling as described previously.

For the simulations of the Holo states, an oxidized nicotinamide adenine dinucleotide and oxamic acid molecule for each monomer were kept in place in the catalytic site using restrains to maintain them in place during the long time evolution of the system. All simulations were carried out using Charmm36 force field (Huang et al., 2017), TIP3P water model2and the GROMACS 2018 Software (Van der Spoel et al., 2005; Abraham et al., 2015). All systems

were simulated in the NPT ensemble at ambient condition, p = 1atm, in a cubic box with zero total charge. For the Apo state, the trajectories were produced at different temperatures: 300, 320, 340 and 350 K, whereas proteins in the Holo states were simulated only at T = 300 K, for comparison. After an initial equilibration phase, at each temperature, the systems were evolved in time for 1 μs with a time step of 2 fs. To analyze the generated trajectories we performed conformational clustering in order to individuate the main protein conformations and their interconversion, and therefore characterize the conformational landscape as a function of the temperature. Daura algorithm (Daura et al., 1999) was chosen to cluster the configurations according to their RMSD. The cut-off used to separate the states depends on the region considered. For instance when focusing on the entire monomer, the cut-off was of 1.7 Å. The analysis of the trajectories also allows to construct the transitions among the individuated conformational states, and therefore it is also possible to aggregate them according to their interconversion kinetics. This clustering procedure allows individuating those conformations that are kinetically separated: configurations that interchange frequently will be clustered in the same kinetic trap. This analysis was performed using the Markov clustering algorithm (Van Dongen, 2000) with a granularity parameter of 1.8. In our analysis, we have considered the entire monomers, and two important sub-sets of amino acids. The first group represents the allosteric hydrophobic core (Alco) defined by the following residues: R148, F149, R150, L153, Y167, V168, L178, W180 for *T. the* LDH and R148, L149, R150, I153, Y167, I168, A178, W180 for *P. mob* LDHs models. The second set, representing the FBP binding site (FBPbs), is defined by R150, H165, Y167, S182, Q184, G186, G187 for *T. the* LDH and R150, H165, Y167, S182, M184,G186, G187 for *P. mob* LDH.

Salt bridges formation was analyzed accordingly to a geometric definition involving distances between selected atoms of charged residues; this allowed identifying ionic pairs that strongly interact among them. Atoms involved in the formation of a salt bridge are -Nitrogen atoms of the side chain of Arg, Lys and His,-Oxygen atoms of the side chain of Asp and Glu. If any of the listed atoms of the positively charged group of residues is closer than 4.0 Å to any other listed atoms of the negatively charged group of residues, there is formation of a salt bridge between the two residues the atoms belong to.

4.8. Primary sequence alignment, structural superpositions and representations

Primary sequences were aligned using MUSCLE (Edgar, 2004).

The structure images were represented with PyMOL (The PyMOL Molecular Graphics System, Version 1.8.6.0 Schrödinger, LLC).

Acknowledgements

The authors acknowledge funding by Agence Nationale de la Recherche (ANR) grant to DM (program AlloAnc ANR-16-CE11-0011) and to EG (program Ln23 ANR-13-BS07-0007-01). This work used the platforms of the Grenoble Instruct-ERIC center (ISBG; UMS 3518 CNRS-CEA-UGA-EMBL) within the Grenoble Partnership for Structural Biology (PSB), supported by FRISBI (ANR-10-INBS-0005-02) and GRAL, financed within the University Grenoble Alpes graduate school (Ecoles Universitaires de Recherche) CBH-EUR-GS (ANR-17-EURE-0003). IBS acknowledges integration into the Interdisciplinary Research Institute of Grenoble (IRIG, CEA). FS acknowledges the financial support by the Initiative d'Excellence program from the French State (Grant DYNAMO, ANR-11-LABX-0011-01, and CACSICE, ANR-11-EQPX-0008). The work was performed using HPC resources from GENCI [CINES, TGCC, IDRIS] (grant X20206818) and from LBT.

Conflict of interest

The authors declare that they have no conflicts of interest with the contents of this article.

Accession numbers

Accession number PDB ID for *P. mobilis* LDH structure: 6H9S

Author contributions

DM and FS conceived the project. DM performed sample preparation and enzymatic measurements; DM and SE conducted crystallization trials. JR performed the diffraction data collection and structure refinement. EG contributed to diffraction data collection and structure refinement. NC constructed protein models using homology modeling. AI and FS performed the molecular simulation. All the authors wrote the manuscript.

References

Abraham, M. J., Murtola. T., Schulz, R., Páll, S., Smith, J. C., Hess, B. & Lindahl, E. (2015). Gromacs: High performance molecular simulations through multi-level parallelism from laptops to supercomputers. *Software X*1, 19-25.

Arai K., Ishimitsu, T., Fushinobu, S., Uchikoba, H., Matsuzawa, H. &Taguchi, H. (2010). Active and inactive state structures of unliganded Lactobacillus casei allosteric L-lactate dehydrogenase. *Proteins* 78, 681-694.

Arai, K., Hishida, A., Ishiyama, M., Kamata, T., Uchikoba, H., Fushinobu, S. et al. (2002). An absolute requirement of fructose 1, 6-bisphosphate for the Lactobacillus casei L-lactate dehydrogenase activity induced by a single amino acid substitution. *Protein. Eng.* 15, 35-41.

Astl, L., Stetz, G. & Verkhivker, G. M. (2020). Allosteric Mechanism of the Hsp90 Chaperone Interactions with Co chaperones and Client Proteins by Modulating Communication Spines of Coupled Regulatory Switches: Integrative Atomistic Modeling of Hsp90 Signaling in Dynamic Interaction Networks. *J. Chem. Inf. Model*. 60, 3616-3631.

Auerbach, G., Ostendorp, R., Prade, L., Korndörfer, I., Dams, T., Huber, R. & Jaenicke, R. (1998). Lactate dehydrogenase from the hyperthermophilic bacterium thermotoga maritima: the crystal structure at 2.1 Å resolution reveals strategies for intrinsic protein stabilization. *Structure*. 6, 769-781.

Berman, H., Henrick, K. & Nakamura, H. (2003). Announcing the worldwide Protein Data Bank. *Nature Struct. Mol. Biol*. 10, 980-980.

Bowman, G. R. & Geissler, P.L. (2012) Equilibrium fluctuations of a single folded protein reveal a multitude of potential cryptic allosteric sites. *Proc. Natl. Acad. Sci. USA*. 109:11681-11686.

Bruzzese, F. J. & Connelly, P.R. (1997) Allosteric properties of inosine monophosphate dehydrogenase revealed through the thermodynamics of binding of inosine 5'-monophosphate and mycophenolic acid. Temperature dependent heat capacity of binding as a signature of ligand-coupled conformational equilibria. *Biochemistry*. 36, 10428-10438.

Burgner, J. W. & Ray, W. J. (1984). On the origin of lactate dehydrogenase induced rate effect. *Biochemistry* 23, 3636-3648.

Chen, V.B., Arendall, W.B., Headd, J.J., Keedy, D.A., Immormino, R.M., Kapral, G.J. et al. (2010). *MolProbity*, all-atom structure validation for macromolecular crystallography. *Acta. Cryst. D.* 66, 12-21.

Clarke, A. R., Wigley, D. B., Chia, W. N., Barstow, D., Atkinson, T. & Holbrook, J. J. (1986). Site-directed mutagenesis reveals role of mobile arginine residue in lactate dehydrogenase

catalysis. *Nature*.324, 699-702.

Clarke, A.R., Wilks, H.M., Barstow, D.A., Atkinson, T., Chia, W.N. & Holbrook, J. J. (1988). An investigation of the contribution made by the carboxylate group of an active site histidine-aspartate couple to binding and catalysis in lactate dehydrogenase. *Biochemistry* 27, 1617-1622.

Colletier, J. P., Aleksandrov, A., Coquelle, N., Mraihi, S., Mendoza-Barberá, E., Field, M. &Madern, D. (2012). Sampling the conformational energy landscape of a hyperthermophilic protein by engineering key substitution. *Mol. Biol. Evol*. 29, 1683-1694.

Coquelle, N., Fioravanti, E., Weik, M., Vellieux, F. & Madern, D. (2007). Activity, Stability and Structural Studies of Lactate Dehydrogenases Adapted to Extreme Thermal Environments. *J. Mol. Biol.* 374, 547–562.

Cowtan, K. (1999). Error estimation and bias correction in phase-improvement calculations. *Acta. Cryst. D.* 55, 1555-1567.

Daura, X., Gademann, K., Jaun, B., Seebach, D., van Gunsteren, W. F. & Mark, A. E. (1999). Peptide folding: When simulation meets experiment. *Angew. Chem. Int.* 38, 236-40.

Davis, I. W., Leaver-Fay, A., Chen, V.B., Block, J. N., Kapral, G. J., Wang, X., Murray, L. W. Arendall, W. B., Snoeyink, J., Richardson, J. S. & Richardson, D. C. (2007). MolProbity: all-atom contacts and structure validation for proteins and nucleic acids. *Nucleic Acids Res* 35, W375-383.

Deng, H., Vu, D. V., Clinch, K., Desamero, R., Dyer, R. B. &Callender, R. (2011). Conformational heterogeneity within the Michaelis complex of lactate dehydrogenase. *J. Phys. Chem. B.* 115, 7670-7678.

Edgar, R. C. (2004). MUSCLE multiple sequence alignment with high accuracy and high throughput. *Nucleic Acids Res*. 32, 1792-1797.

Engilberge, S., Riobé, F., DiPietro, S., Lassalle, L., Coquelle, N., Arnaud, C. A, et al. (2017). Crystallophore, a versatile lanthanide complex for protein crystallography combining nucleating effects, phasing properties, and luminescence. *Chem. Sci.* 8, 5909-5917.

Engilberge, S., Riobé, F., Wagner, T., Pietro, S.D., Breyton, C., Franzetti, B., Shima, S., Girard, E., Dumont, E. &Maury, O. (2018). Unveiling the Binding Modes of the Crystallophore, a Terbium-based Nucleating and Phasing Molecular Agent for Protein Crystallography. *Chemistry*. 24, 9739-9746.

Eventoff, W., Rossmann, M. G.,Taylor, S. S., Torff, H. J., Meyer, H., Keil, W. &Kiltz, H. H. (1977). Structural adaptations of lactate dehydrogenase isozymes. *Proc. Natl. Acad. Sci. USA* 74, 2677-2268.

Fago, A., Hundahl, C., Dewilde, S., Gilany, K., Moens, L. & Weber, R. E. (2004). Allosteric regulation and temperature dependence of oxygen binding in human neuroglobin and cytoglobin. Molecular mechanisms and physiological significance. *J. Biol. Chem*. 279, 44417-44426.

Feldman-Salit, A., Hering, S., Messiha, H. L, Veith, N., Cojocaru, V., Sieg, A., et al. (2013). Regulation of the activity of lactate dehydrogenases from four lactic acid bacteria. *J. Biol. Chem.* 288:21295-21306.

Fersht, A. (1985). Enzyme structure and mechanism, 2nd edition. Freeman and Co., New york.

Halgand, F., Houée-Lévin, C., Weik, M. &Madern, D. (2020). Remote oxidative modifications induced by oxygen free radicals modify T/R allosteric equilibrium of a hyperthermophilic lactate dehydrogenase. *J. Struct. Biol.* 210, 107478.

Holbrook, J.J., Liljas, A., Steindel, S.J. & Rossmann, M.G. (1975) Lactate Dehydrogenase. in: The Enzymes (Boyer, P.D., ed.), 3rd Edn. Academic Press, New York, pp. 191-292.

Huang, J., Rauscher, S., Nawrocki, G., Ran, T., Feig, M., de Groot, B.L., et al. (2017). CHARMM36m: an improved force field for folded and intrinsically disordered proteins. *Nat. Methods*. 14, 71-73.

Ikehara, Y., Arai, K., Furukawa, N., Ohno, T., Miyake, T., Fushinobu, S., Nakajima, M., Miyanaga, A. & Taguchi, H. (2014). The Core of Allosteric Motion in *Thermus caldophilus* l-Lactate Dehydrogenase. *J. Biol. Chem*. 289, 31550-31564.

Iwata, S., Kamata, K., Yoshida, S., Minowa, T. & Ohta, T. (1994). T and R states in the crystals of bacterial L-lactate dehydrogenase reveal the mechanism for allosteric control. *Nat. Struct. Biol*. 1, 176-185.

Kabsch, W. (2010). XDS. *Acta Crystallogr. D*. 66,125–132.

Kalimeri, M., Rahaman, O., Melchionna, S. & Sterpone, F. (2013). How conformational flexibility stabilizes the hyperthermophilic elongation factor G-domain. *J. Phys. Chem. B.* 117, 13775-13785.

Karshikoff, A., Nilsson, L. & Ladenstein, R. (2015). Rigidity versus flexibility: the dilemma of understanding protein thermal stability. FEBS J. 282, 3899-3917.

Katava, M., Kalimeri, M., Stirnemann, G. & Sterpone, F. (2016). Stability and Function at High Temperature. What Makes a Thermophilic GTPase Different from Its Mesophilic Homologue.*J Phys Chem B*. 120, 2721-2730.

Katava, M., Maccarini, M., Villain, G. et al. (2017). Thermal activation of 'allosteric-like' large-scale motions in a eukaryotic Lactate Dehydrogenase. *Sci Rep*. 7, 41092.

Katava, M., Marchi, M., Madern, D., Sztucki, M., Maccarini, M. &Sterpone, F. (2020) Temperature Unmasks Allosteric Propensity in a Thermophilic Malate Dehydrogenase via Dewetting and Collapse. *J. Phys. Chem. B.* 124, 1001-1008.

Kim, J., Ahuja, L. G., Chao, F.A., Xia, Y., McClendon, C. L., Kornev, A. P., et al. (2017). A dynamic hydrophobic core orchestrates allostery in protein kinases. *Sci. Adv*. 3,e1600663.

Kolappan, S., Shen, D. L., Mosi, R., Sun, J., McEachern, E. J., Vocadlo, D.J. & Craig, L. (2015). Structures of lactate dehydrogenase A (LDHA) in Apo, ternary and inhibitor-bound forms. *Acta Crystallogr D Biol Crystallogr*. 71, 185-195.

Koshland, D.E. Jr., Némethy, G. & Filmer, D. (1966) Comparison of experimental binding data and theoretical models in proteins containing subunits. *Biochemistry*. 5, 365-385.

Lien, T., Madsen, M., Rainey, F. A. & Birkeland, N. K. (1988). Petrotoga mobilis sp. nov., from a North Sea oil-production well. *Int. J. Syst. Bacteriol*. 48, 1007-1013.

Lisi, G. P., Currier A. A. & Loria, J. P. (2018). Glutamine Hydrolysis by Imidazole Glycerol Phosphate Synthase Displays Temperature Dependent Allosteric Activation. *Front. Mol. Biosci*. 5, 4.

Maffucci, I., Laage, D., Stirnemann, G. & Sterpone, F. (2020). Differences in thermal structural changes and melting between mesophilic and thermophilic dihydrofolate reductase enzymes. *Phys Chem Chem Phys*. 22, 18361-18373.

Matoba, Y., Miyasako, M., Matsuo, K., et al. (2014). An alternative allosteric regulation mechanism of an acidophilic l-lactate dehydrogenase from Enterococcus mundtii 15-1A. *FEBS Open Bio*. 4, 834-847.

McCoy, A. J., Grosse-Kunstleve, R. W., Adams, P. D., Winn, M. D., Storoni, L. C. & Read, R. J. (2007). *Phaser* crystallographic software. *J. Appl Cryst*. 40, 658-674.

Monod, J., Wyman, J. & Changeux, J. P. (1965). On the nature of allosteric transitions, a plausible model. *J. Mol. Biol*. 12, 88-118.

Motlagh, H. N., Li, J., Thompson, E. B. & Hilser, V. J. (2012). Interplay between Allostery and Intrinsic Disorder in an Ensemble. *Biochem. Soc. Trans.*40, 975– 980.

Motlagh, H. N., Wrabl, J. O., Li, J. & Hilser, V. J. (2014). The ensemble nature of allostery.Nature 508, 331-339.

Oshima, T. & Imahori, K. (1975). Description of Thermus thermophilus (Yoshida and Oshima) comb. nov., a Nonsporulating Thermophilic Bacterium from a Japanese Thermal Spa. *Int. J. Syst. Bacterio*. 24,102-112.

Painter, J. & Merritt, E. A. (2005). A molecular viewer for the analysis of TLS rigid-body motion in macromolecules. *Acta Cryst. D*. 61, 465-471.

Painter, J. & Merritt, E. A. (2006). Optimal description of a protein structure in terms of multiple groups undergoing TLS motion. *Acta Cryst. D*. 62, 439-450.

Peng, H. L., Egawa, T., Chang, E., Deng, H. & Callender, R. (2015). Mechanism of Thermal Adaptation in the Lactate Dehydrogenases. *J. Phys. Chem. B.* 119, 15256-15262.

Piontek, K., Chakrabarti, P., Schär, H.P., Rossmann, M. G. & Zuber H. (1990). Structure determination and refinement of Bacillus stearothermophilus lactate dehydrogenase. *Proteins*. 7, 74-92.

Rajasekaran, N., Suresh, S., Gopi, S., Raman, K. & Naganathan, A. N. (2017). A General Mechanism for the Propagation of Mutational Effects in Proteins. *Biochemistry*. 56, 294-305.

Rossmann, M.G., Adams, M.J., Buehner, M., Ford, G. C., Hackert, M.L., Liljas, A., et al. (1973). Letter: Molecular symmetry axes and subunit interfaces in certain dehydrogenases. *J. Mol. Biol*. 76, 533-537.

Schrank, T.P., Bolen, D. W. & Hilser, V. J. (2009). Rational modulation of conformational fluctuations in adenylate kinase reveals a local unfolding mechanism for allostery and functional adaptation in proteins. *Proc. Natl. Acad. Sci. USA*. 106, 16984-16989.

Schroeder, G., Matsuzawa, H. & Ohta, T. (1988). Involvement of the conserved histidine-188 residue in the L-lactate dehydrogenase from Thermus caldophilus GK24 in allosteric regulation by fructose 1, 6-bisphosphate. *Biochem Biophys Res Commun.* 152, 1236-1241.

Sitzia, F, Brown, J. T, Randall, A. D. & Dunlop, J. (2011) Voltage- and Temperature-Dependent Allosteric Modulation of α7 Nicotinic Receptors by PNU120596. *Front. Pharmacol*. 2, 81.

Sterpone, F. & Melchionna, S. (2012). Thermophilic proteins: insight and perspective from in silico experiments. *Chem Soc Rev*. 41, 1665-1676.

Sterpone, F., Bertonati, C., Briganti, G. & Melchionna, S. (2009). Key role of proximal water in regulating thermostable proteins. *J Phys Chem B*. 113, 131-137.

Swain, J. F. & Gierasch, L. M. (2006). The Changing Landscape of Protein Allostery. *Curr. Opin. Struct. Biol. 16*, 102– 108.

Taguchi, H. (2017). The Simple and Unique Allosteric Machinery of Thermus caldophilus Lactate Dehydrogenase: Structure-Function Relationship in Bacterial Allosteric LDHs. *Adv. Exp. Med. Biol.* 925, 117-145.

Van Der Spoel, D., Lindahl, E., Hess, B., Groenhof, G., Mark, A. E. & Berendsen, H. J. (2005). GROMACS: fast, flexible, and free. *J. Comput. Chem*. 26, 1701-1718.

Van Vliet, F., Xi, X. G., De Staercke, C., de Wannemaeker, B., Jacobs, A., Cherfils, J., et al. (1991). Heterotropic interactions in aspartate transcarbamoylase: turning allosteric ATP

activation into inhibition as a consequence of a single tyrosine to phenylalanine mutation. *Proc. Natl. Acad. Sci. USA*. 88, 9180-9183.

Van Dongen, S. M. (2000). Graph Clustering by Flow Simulation. Ph.D Thesis, University of Utrecht, The Netherlands.

Waterhouse, A., Bertoni, M., Bienert, S., Studer, G., Tauriello, G., Gumienny, R., Heer, F.T., de Beer, T. A. P., Rempfer, C., Bordoli, L., Lepore, R. & Schwede, T. (2018). SWISS-MODEL: homology modelling of protein structures and complexes. *Nucleic Acids Res*. 46, W296-W303.

Wei, G., Xi, W., Nussinov, R. & Ma, B. (2016). Protein Ensembles: How Does Nature Harness Thermodynamic Fluctuations for Life? The Diverse Functional Roles of Conformational Ensembles in the Cell. *Chem. Rev*. 116, 6516-6551.

Wigley, D. B., Gamblin, S. J., Turkenburg, J. P, Dodson, E. J., Piontek, K., Muirhead, H., & Holbrook, J. J. (1992). Structure of a ternary complex of an allosteric lactate dehydrogenase from Bacillus stearothermophilus at 2.5 A resolution. *J. Mol. Biol*. 223, 317-335.

Winter, V. J., Cameron, A., Tranter, R., Sessions, R. B. & Brady, R. L. (2003). Crystal structure of Plasmodium berghei lactate dehydrogenase indicates the unique structural differences of these enzymes are shared across the Plasmodium genus. *Mol Biochem Parasitol*. 131, 1-10.

Wodak, S. J., Paci, E., Dokholyan, N. V., Berezovsky, I. N, Horovitz, A., Li, J., et al. (2019). Allostery in Its Many Disguises: From Theory to Applications. Structure. 27, 566-578.

Yang, J. & Zhang, Y. (2015). I-TASSER server: new development for protein structure and function predictions. *Nucleic Acids Res.* 43, W174-181.

Figures captions.

Figure 1. Enzymatic activity profiles for pyruvate. (A, B, C and D) *P. mob* LDH.(E, F, G and H) *T. the* LDH. The scale for pyruvate concentration is logarithmic. (A, B, E and, F) measurements done at 50°C. (C, D, G and H) measurements done at 70°C. (B, D, F and H) activity profiles in the presence of 3 mM FBP.

Figure 2. Structure of the tetrameric *P. mob* LDH. (A) Cartoon representation of the four monomers are labeled A to D. Chains are colored in "chainbow" mode. Subunits of the tetrameric assembly are related by three molecular dyads, *P*, *Q* and *R*. (B) *P. mob* LDH

monomer representation. α-helices are colored in orange whereas β-strands and loops are in green and red, respectively. Arrows indicate two small areas not built in the final model.

Figure 3. Structural comparison between *P. mob* and Apo *T. the* LDH (2V6M). (A) Close up view of interface between monomers A and D of *P. mob* LDH. The P-axis showing the symmetry is indicated by a blue circle. Amino acids involved in the various area that are discussed in the main body of the manuscript are shown in spheres of different colors. With *P. mob* LDH, the numbering corresponds to the primary sequence, whereas in *T. the* LDH the structural numbering is used (Eventoff et al., 1977). The allosteric core of monomer A (Alco (A)) and monomer D (Alco (D)) are colored in green and yellow, respectively. The dashed line indicates area of monomer A and monomer D that are involved in the FBPbs. Corresponding amino acids are colored in pale green and pale yellow, respectively. H165 that also belong to the FBPbs are in orange. Substrate binding residuesR148 are in red spheres. (B) Close up view of *P. mob* LDH showing R148(A)in the conformational sub-state outside the catalytic site. The neighboring residue H47 from adjacent monomer B is also shown. (C) Same view for *T. the* LDH.(D) Close up view of the Alco of monomer A in *P. mob* LDH. To illustrate contacts between residues, the van der Wall surface is depicted. (E) Same view for *T. the* LDH.(F and G) Close up view of AD interfaces in *P. mob* and *T. the* LDHs, respectively. (H and I) Close up views of important histidine residues involved in FBPbs of *P. mob* and *T. the* LDHs, respectively.

Figure 4. Effect of temperature on the conformational landscape of *T. the* and *P. mob* LDHs. (A) Graphs representation of the configurational clusters of the monomer D for each enzyme at two representative temperatures (300 K and 340 K). The size of the nodes is proportional to the population of the cluster. Nodes are colored according to the RMSD value of the centroid of each cluster from the configuration of the protein in the Apo state after the equilibration phase at 300 K and they are spatially arranged according to the result of kinetic clustering procedure. Color scale from blue to red corresponds to increasing RMSD. (B) Average number of configurational asymptotic clusters, $\langle N_\infty \rangle$, and kinetic clusters, $\langle N_K \rangle$, as a function of temperature. For each LDH the value is obtained as an average over the four domains. Insets report the same values in linear log scale, superimposed dashed lines are best fits with an exponential law.

Figure 5. Thermal dependent fluctuations of the substrate binding residue R148(171) for *P. mob* LDH (A) and *T. the* LDH(B). The conformational space sampled by R148(171) is projected in the two-dimensional space defined by the RMSD with respect to the Apo ($RMSD_A$) and Holo ($RMSD_H$) states of the residue in homology models or X-ray structures. Color scale from blue to red indicates values with increasing density. The density distributions are sampled at 300 K and 340 K. The inset panels represent local conformations of R148(R171) and its surrounding environment for representative states.

Figure 6. Effect of temperature on the allosteric core and the FBP binding site (FBPbs) of *P. mob* and *T. the* LDHs. (A and C) Results of the clustering analysis for the Alco and FBPbs of domain D. Graphs represent the configurational clusters for each enzyme at the lowest and highest temperature investigated (300 K and 340 K, respectively). The size of the nodes is proportional to the population of the cluster. Nodes are colored according to the RMSD value of the centroid of each cluster from the configuration of the protein in their Apo state after the equilibration phase at 300 K and they are spatially arranged according to the result of kinetic clustering procedure. (B and D) Average number of configurational asymptotic clusters, $<N\infty>$, and kinetic clusters, $< N_K>$, as a function of temperature. For each LDH the value is obtained as an average over the four domains. Insets report the same values in linear-log scale, superimposed dashed lines are best fits with an exponential law.

Figure 7. Effect of temperature on H165(188) packing. (A) Probability distributions of the distances between Cγ atoms of H165(188) of monomers A and D and B and C for the APO simulations at 300 K and 340 K. Orange and green dashed lines correspond respectively to histidine pairs distances representative of R-active and T-inactive states.(B) Ribbon drawing of the *P. mob* LDH. H165(188) is highlighted accordingly to color codes for monomers A, B, C and D.

Figure 8. Structural features relating the thermal dependent conformational dynamics of *P. mob* (brown) and *T. the* (green) LDHs. (A) Propensity of the substrate-binding residue R148(171) to sample the R-active and T-inactive like states. (B) Capability of the rigid allosteric core to propagate mechanical signal induced by temperature: fuzzy in *P. mob* compared to straightforward in *T. the* LDH. The shape of the conformational basins are

schematized. (C) Communication between the domain interfaces in each LDH upon thermal excitation or addition of FBP. Open stars (weak interaction), plain stars (strong interaction).

	P. mob LDH				*T. the LDH*			
Tre (°C)	50	70	50 +FBP	70 +FBP	50	70	50 +FBP	70 +FBP
V_{max} (U/mg)			240	939	90	345	109	433
K_m (mM)			0.65	0.17	0.24	0.11	0.09	0.09
V_{max}/K_m ($min^{-1}.mg^{-1}$)			369	5523	375	3136	1211	4811

Table1. Kinetic parameters of *P. mob* and *T. the* LDHs for pyruvate.

Figure. 1.

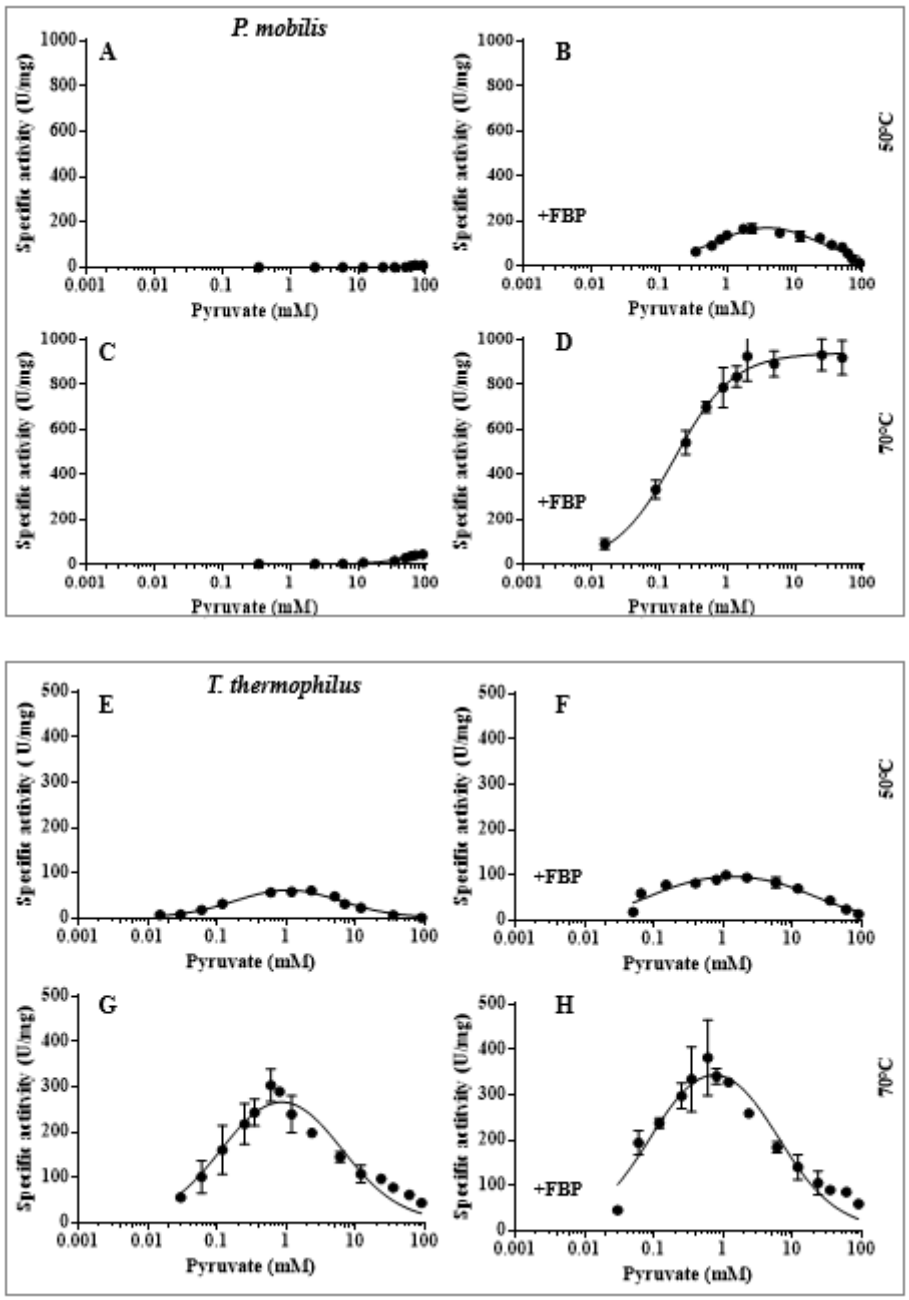
P. mobilis
A
B
C
D
+FBP
50°C
70°C
Specific activity (U/mg)
Pyruvate (mM)
T. thermophilus
E
F
G
H
Specific activity (U/mg)

Figure 2.

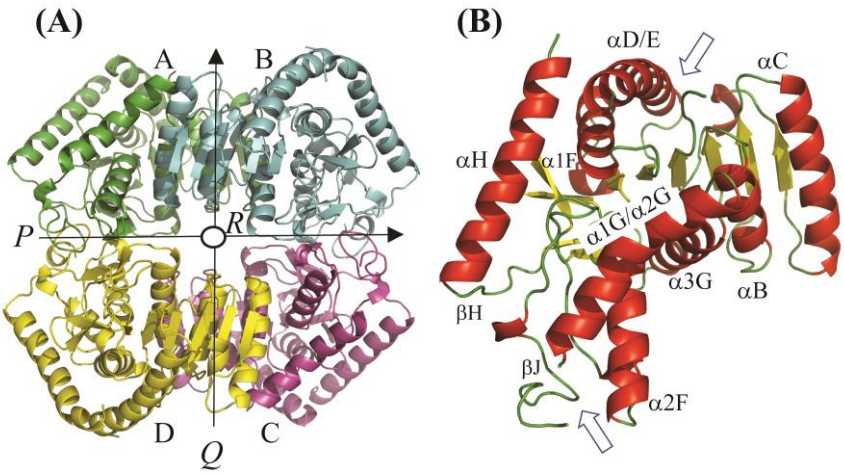

Figure 3.

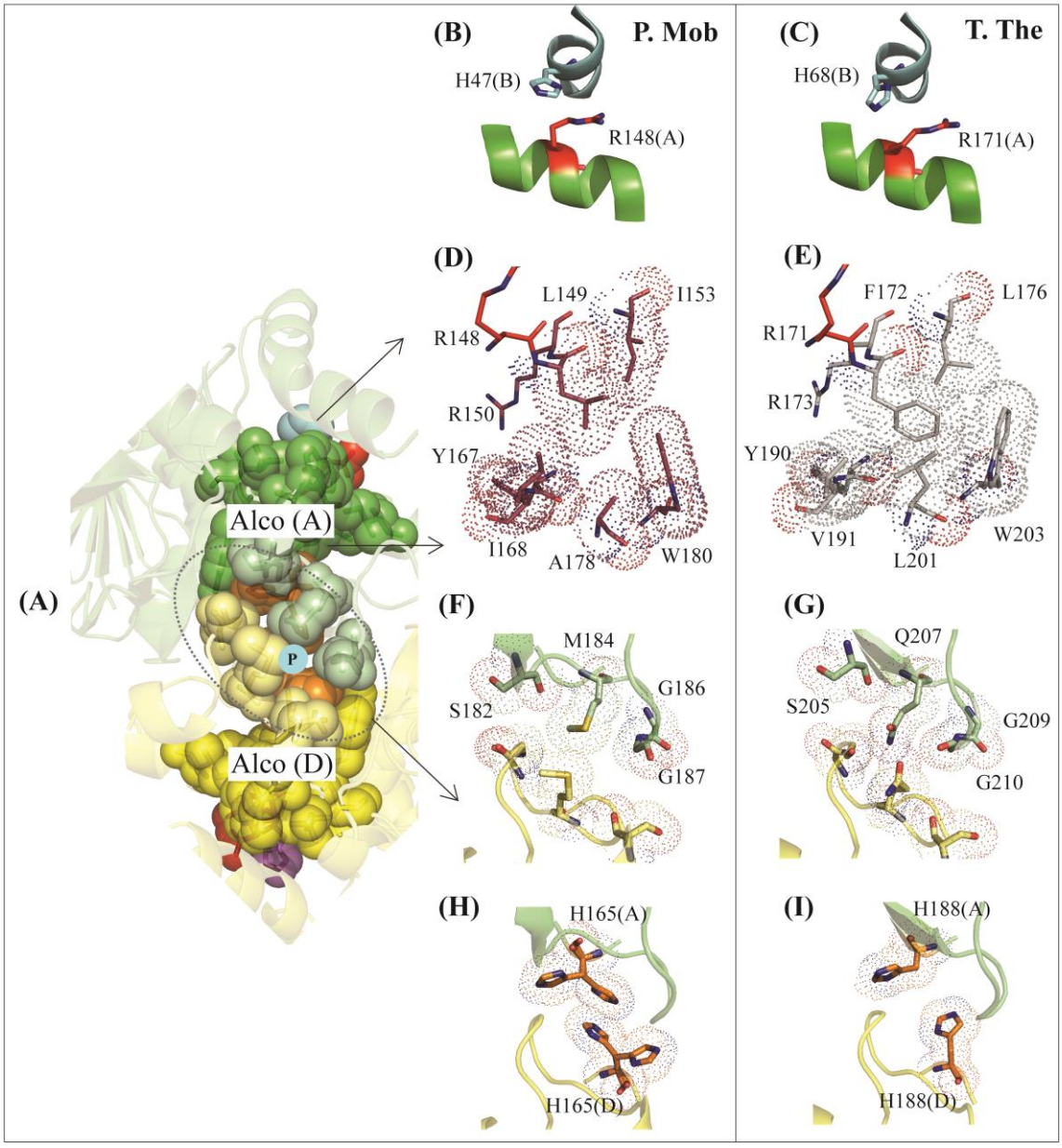
(A)
Alco (A)
Alco (D)
P
(B)
P. Mob
H47(B)
R148(A)
(C)
T. The
H68(B)
R171(A)
(D)
L149
I153
R148
R150
Y167
I168
A178
W180
(E)
F172
L176
R171
R173
Y190
V191
L201
W203
(F)
M184
G186
S182
G187
(G)
Q207
S205
G209
G210
(H)
H165(A)
H165(D)
(I)
H188(A)
H188(D)

Figure 4.

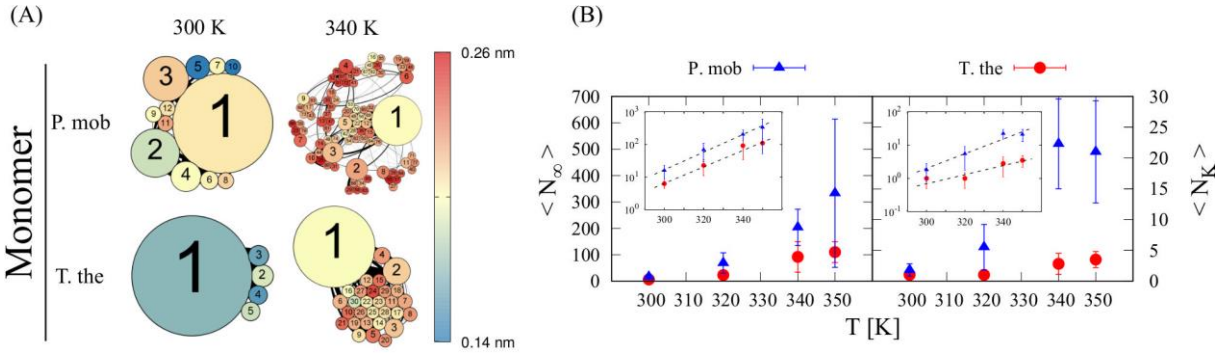

Figure 5.

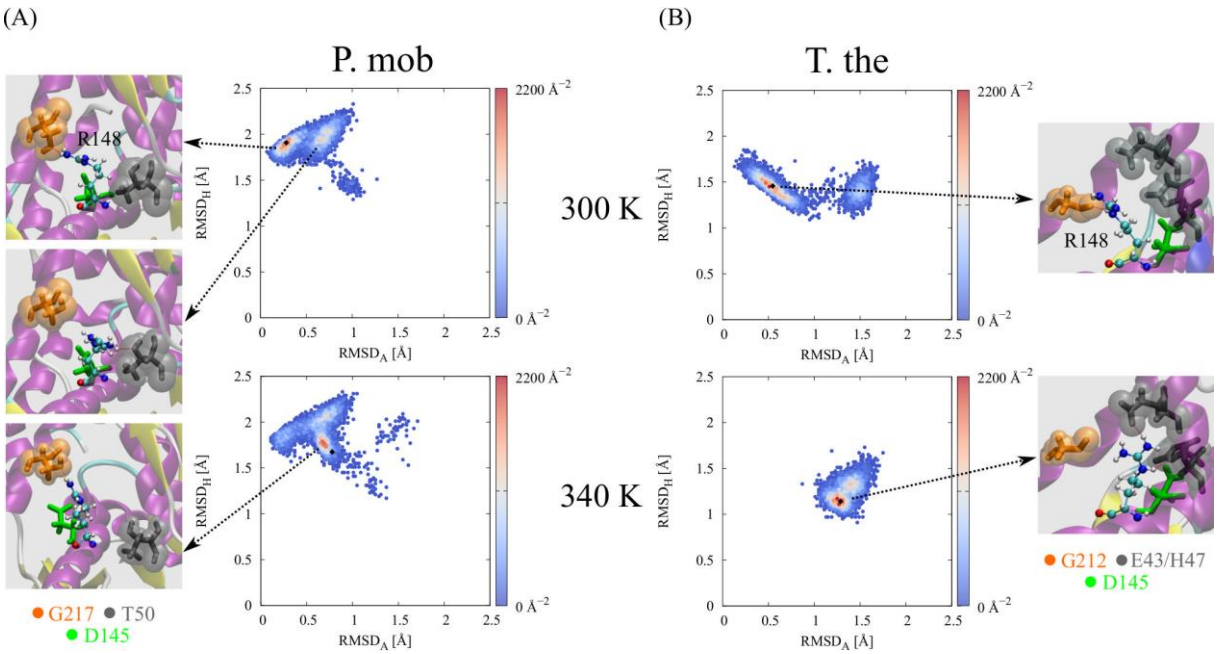

Figure 6.

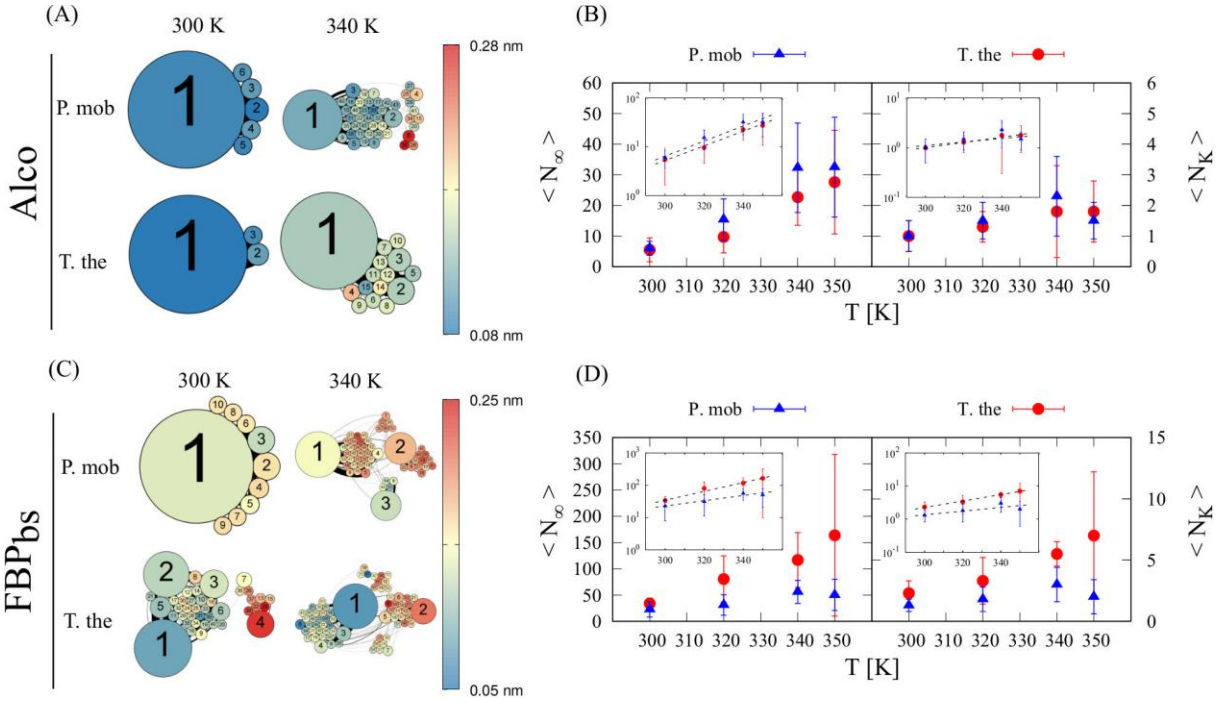

Figure 7.

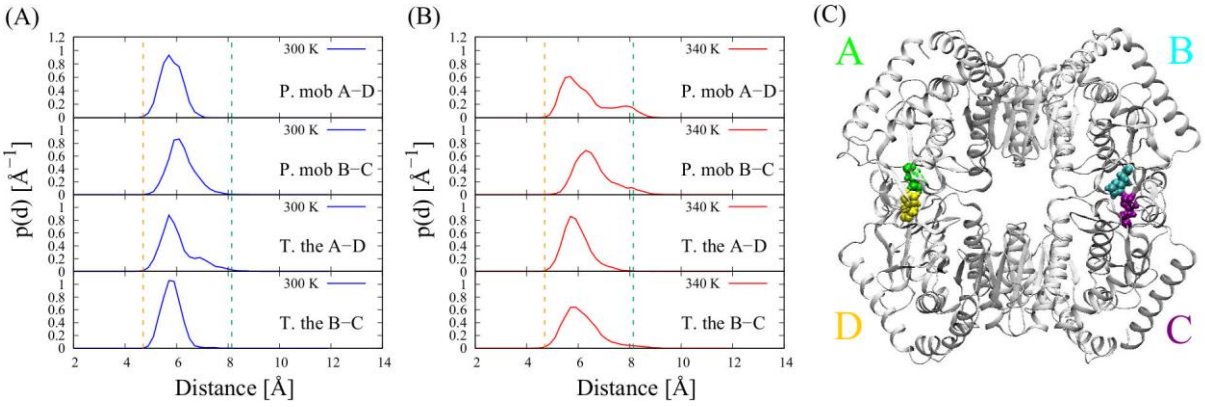

Figure 8.

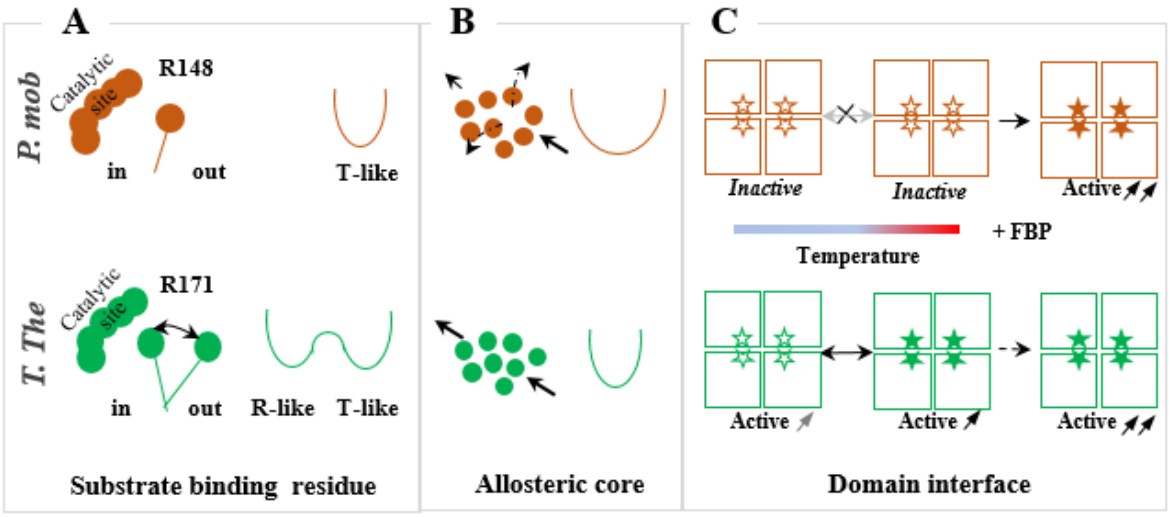
A
B
C
P. mob
Catalytic site
R148
in
out
T-like
T. The
Catalytic site
R171
in
out
R-like
T-like
Substrate binding residue
Allosteric core
Inactive
Inactive
Active
+ FBP
Temperature
Active
Active
Active
Domain interface